Fusion and binary reactions in the collision of ^{32}S on ^{26}Mg at $E_{lab}=163.5$ MeV

Salvatore Cavallaro and Yin Shu Zhi*
Dipartimento di Fisica dell'Universitá di Catania, and Laboratorio Nazionale del Sud, I-95129 Catania, Italy

Gianfranco Prete
Laboratori Nazionali di Legnaro, I-35020 Legnaro, Padova, Italy

Giuseppe Viesti
Dipartimento di Fisica dell'Universitá di Bari, I-70126 Bari, Italy
(Received 13 March 1989)

Measurements of heavy fragments produced in the interaction of ^{32}S with ^{26}Mg at $E_{lab}=163.5$ MeV have been performed to study the interplay of the fusion reaction and binary processes. Experimental angular distributions, velocity spectra, and angle-integrated cross sections of detected heavy fragments have been compared with predictions of statistical models. The comparison shows that complete fusion exhausts the production of residues in the range $Z=26-22$. For fragments with atomic number $Z=21$ and $Z=20$ some other mechanism is also present. The analysis of energy spectra, angular distributions, and total kinetic energy of projectile-like fragments ($Z=19-6$) shows that the main process to limit fusion is an inelastic mechanism with large energy damping.

I. INTRODUCTION

The fusion of heavy ions in the mass region $A_1+A_2\sim 60$ has recently been extensively studied for energies near and above the Coulomb barrier.[1-5] The bombarding energy dependence of the fusion cross section is generally described by defining three energy domains which clearly emerge from experimental data. In the first domain, the fusion cross section shows an almost linear behavior as a function of $1/E_{c.m.}$ which depends on the static fusion barrier determined by the interplay of nuclear, Coulomb, and centrifugal forces. As long as the projectile energy is able to overcome the barrier, fusion occurs and exhausts the major part of the reaction cross section (regime I). For bombarding energies well above the fusion threshold, the fusion cross section is seriously limited, although it is still an increasing function of the beam energy (regime II). At higher energies, it has been observed that σ_{fus} decreases with $1/E_{c.m.}$, due to some instability of the composite system (regime III). The last two energy ranges are characterized by the competition between the fusion and other damped reaction mechanisms (deep inelastic, incomplete fusion, dynamical fission). Several models try to account for the limitation to the fusion as an effect related to the entrance channel[6-9] or to the structure of the compound nucleus.[10-13].

A large amount of experimental work has been devoted to clarifying the limitation of the fusion process and studying the characteristics of the competing reaction mechanisms. In fact, detailed information on these phenomena can give correct scaling of physical parameters (interaction times, critical distances, angular momenta involved, strength of friction forces), allowing a better understanding of the nucleus-nucleus collisions.

From an experimental point of view, fissionlike and deep-inelastic contributions have been evidenced for $A_{CN}\sim 60$ systems [$^{20}Ne+^{27}Al$ at $E_{lab}=120$ MeV (Ref. 1), $^{16}O+^{40,44}Ca$ at $E_{lab}=70-87$ MeV (Ref. 14), and $^{32}S+^{50}Ti$ at $E_{lab}=120-170$ MeV (Ref. 15)]. In other cases only deep-inelastic and quasielastic contributions have been indicated as main mechanisms in competition with fusion [$^{32}S+^{27}Al$ at $E_{lab}=140-390$ MeV (Ref. 16), $^{20}Ne+^{20}Ne$ at $E_{lab}=80-160$ MeV (Ref. 17), and $^{16}O+^{48}Ti$ at $E_{lab}=100$ MeV (Ref. 18)]. For the reaction $^{20}Ne+^{26}Mg$ at $E_{lab}=150$ MeV, an incomplete fusion reaction has also been identified.[2]

We measured, in the past, the fusion cross section of ^{32}S with $^{24,25,26}Mg$ at bombarding energies of 90–150 MeV using in-beam γ-ray techniques and, for the highest beam energies, we showed the onset of regime II, where the competition between fusion and binary processes is supposed to become effective.[19] Therefore, it seemed interesting to us to perform direct measurements of the reaction products with the aim of investigating the competition between fusion and other reaction mechanisms in the S+Mg systems.

We report here on a study of reaction products from the $^{32}S+^{26}Mg$ reaction at $E_{beam}=165$ MeV. Energy spectra and angular distributions of fragments with atomic number ranging from the fusion region ($Z=26-21$) to the extreme limits of binary reactions ($Z=20-6$) have been measured and analyzed with the aid of statistical-model calculations and phenomenological models of deep-inelastic reactions.

II. EXPERIMENTAL METHODS

The experiment was performed at the XTU-Tandem facility of Laboratori Nazionali di Legnaro. The beam of ^{32}S ions ($q=11^+$) at an energy of 165 MeV was used. Beam current values were in the range 30–100 nA. The bombarded targets consisted of self-supporting Mg, with

a composition of 97.2% on $A=26$, 1.7% on $A=24$, and 1.1% on $A=25$ isotopes, respectively. Evaporation of a thin ^{197}Au layer on the target was previously made for normalization purposes. The Mg and Au thickness was determined by backscattering of α particles at the V.D.G. accelerator of the Physics Department of Catania University. The measured values are 365 ± 20 μg/cm^2 and 270 ± 15 μg/cm^2 for the two Mg targets used and 9.5 ± 0.5 μg/cm^2 for the gold layer. Carbon and oxygen contamination was previously estimated[19] to be as low as ~15 μg/cm^2.

Heavy fragments ($Z=26-13$) were detected by a Bragg ionization chamber (BIC) in the angular range $\theta_{lab}=7°-20°$ with a step $\Delta\theta_{lab}=2°$. The BIC was connected with a sliding-seal scattering chamber at a distance of 41.5 cm from the target. Rectangular slits (5×25 mm^2) defined the acceptance of the detector to be $\Delta\Omega=0.73$ msr. The Bragg ionization chamber is fully described in Ref. 20. In this work the entrance window was 1 μm thick Mylar foil. P10 at a pressure of 180 Torr was used as counting gas.

The Z-discrimination power of the BIC was good enough to discriminate very clearly each element in the range $Z=3-26$, with the exception of low-energy saturation and high-energy punch through for $Z\leq10$ fragments. Energy spectra for elements in the fusion-evaporation region have been derived by means of linearization, and discrimination was operated for the low-energy saturated part of the energy spectra.

Lighter fragments ($Z\leq20$) were also detected by two ΔE-E telescopes ($\Delta E=10$ μm and $E=500$ μm thick solid-state silicon detectors) in the angular range $\theta_{lab}=13°-70°$ with a step $\Delta\theta_{lab}=2°$. They were put at a distance of 16 cm from the target covering a solid angle of $\Delta\Omega=0.49$ msr.

Two solid-state detectors were also placed at $\theta_{lab}=\pm20°$ with respect to the incident beam for monitoring. Beam intensity was also collected by a Faraday cup system and integrated by a suitable charge integrator module. To normalize the beam charge measured by the Faraday cup integration setup, we used the elastic scattering of the ^{32}S on the ^{197}Au thin film present in the target averaged over the $\theta_{lab}=7°-11°$ measurements. Considering the uncertainties related to target thickness, beam integration, and angular position of the detectors, an overall error of 17% is attributed to the absolute value of the differential cross section reported in this work, whenever statistical error contribution can be neglected.

III. FUSION REACTION

In this section, experimental results for fragments in the evaporation residue region are shown and compared with the prediction of statistical-model calculations from the codes LILITA (Ref. 21) and CASCADE (Ref. 22). For velocity spectra and angular distributions we used LILITA, which computes differential cross sections by the Monte Carlo method. Integrated cross sections are compared with results from both codes.

Standard input parameters to the statistical models were used. To derive the level densities at low excitation energy, experimental levels, including those coming from heavy-ion gamma spectroscopy, were used. Within the sharp cutoff model, the transmission coefficients in the entrance channel are assumed to be equal to 1 until a critical value of the angular momentum l_{cr} is reached. Quantum-mechanical effects are taken into account by introducing a diffuseness parameter $\Delta=1\hbar$ which produces a spreading effect on the transmission probability for angular momentum values near l_{cr}. The critical angular momentum was fixed at the value of $l_{cr}=35\hbar$, following the results of Ref. 23.

Experimental angular distributions $(d\sigma/d\omega)_{lab}$ for $Z=25-20$ are shown in Fig. 1 compared with LILITA statistical-model calculations. The experimental data show the well-known forward peaking with a width which increases going from $Z=25$ to $Z=21$. For $Z=20-17$ a large-angle component appears clearly, giving evidence for the onset of another reaction mechanism different from fusion. Data for $Z=26$ are not reported because these cross sections are negligible except for the

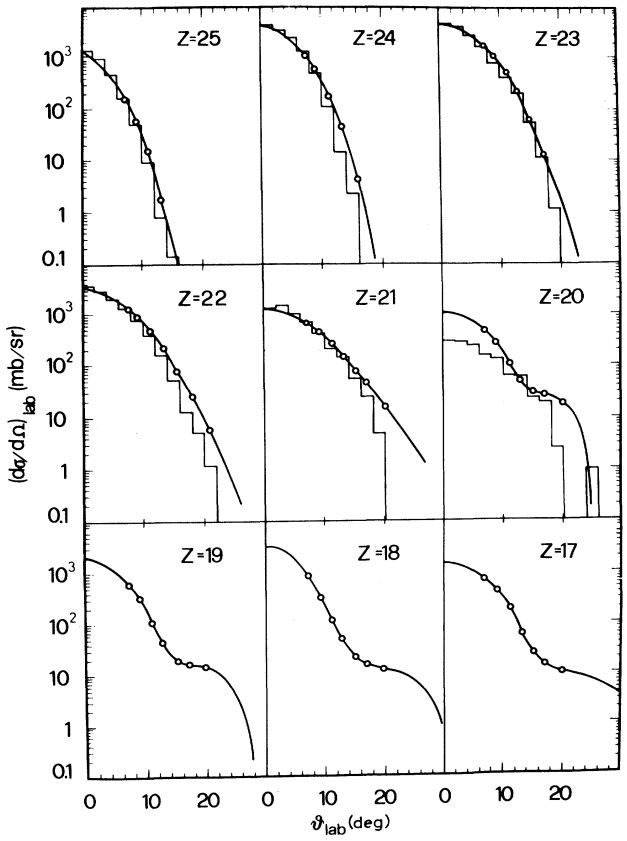

FIG. 1. Angular distributions of fragments with $Z=25-20$. Continuous lines have been used to integrate cross sections. Histograms are predictions from the LILITA statistical-model calculations.

most forward angles.

Solid lines in Fig. 1 have been used for interpolation between experimental data in computing the angle-integrated cross sections $\sigma(Z)$. Histograms represent the LILITA predictions normalized to the experimental values. The shape of angular distributions for fragments with $Z=25-21$ is very well reproduced by the statistical-model calculations. For fragments with $Z=20$, deviations between the experimental data and the model calculations are present.

To obtain clearer information about the Z range effectively contributing to the complete fusion we have converted the energy spectra into velocity distributions and compared those with the model prediction. Whenever a complete fusion event occurs, light particles are emitted in the frame of the recoiling nucleus with angular distribution symmetric around 90° and Maxwellian energy spectra. If angular distributions of particles are assumed to be isotropic, the velocity distributions of the evaporation residue can be expressed in the form of invariant cross section as[24,25]

$$\frac{1}{V_R^2}\frac{d^2\sigma}{d\Omega_R dV_R}=ke^{-V_C^2\sin^2(\theta_L)/2s^2}e^{-[V_R-V_c\cos(\theta_L)]^2/2s^2}, \tag{1}$$

where k is a normalization constant, V_C and θ_L are, respectively, the velocity of the compound nucleus and the detection angle of the residue in the laboratory frame, and s is the standard deviation from the mean recoil velocity which depends on the complexity of the evaporation cascade.

From Eq. (1) it appears that the velocity distribution at fixed detection angle θ_L has a Gaussian shape with centroid

$$V_R=V_C\cos\theta_L \tag{2}$$

and width s. Anisotropic angular distributions of evaporated particles change the shape of the residue velocity spectra, so that Eq. (1) is no longer valid, but Eq. (2) still holds. Therefore, by inspecting the velocity spectrum one can immediately check the presence of the complete

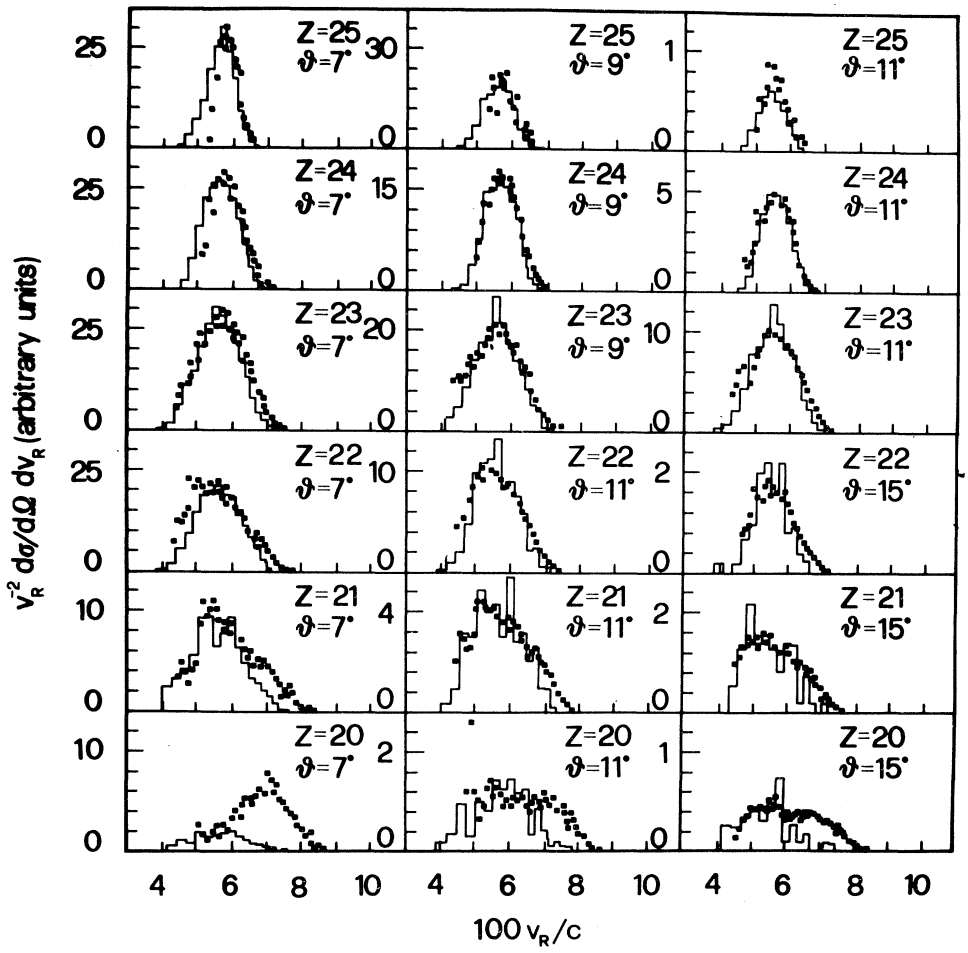

FIG. 2. Samples of velocity spectra of fragments with $Z=25-20$. Histograms are predictions from the LILITA statistical-model calculations.

fusion mechanism.

Samples of the experimental velocity spectra are reported in Fig. 2. To transform the measured energy into velocity of a given Z residue, mean mass values from the measurements of in-beam γ rays have been used.[26] The experimental spectra for $Z=25-21$ show symmetric shapes and peak at velocity $V_R/c=5-6\times10^{-2}$, well in agreement with values from Eq. (2).

The velocity distributions for $Z=20$ present structures at high velocity, and the peak position is far from that expected in the case of complete fusion. Velocity spectra from the LILITA code are also shown by histograms in Fig. 2. The statistical model works very well in reproducing the velocity distributions for fragments with $Z=25-21$.

Figure 3 reports samples of experimental spectra for fragments with $Z=20-17$ to show the trend of the experimental velocity distributions for lighter fragments. It appears that the velocity distributions peak far from the values expected from Eq. (2) in the case of complete fusion (thick arrows in Fig. 3). The maximum of the distributions at $\theta_{lab}=20°$ moves to higher velocity values as the fragment Z decreases, overcoming the velocity corresponding to the Coulomb repulsion energies for binary fragmentation of the compound system.

Low-energy thresholds in the experimental spectra of Figs. 2 and 3 are due to the saturation of the Bragg detector Z-identification signal. This effect has been corrected when integrating the cross sections.

In Fig. 4 the measured elemental distribution $\sigma(Z)$ of fragments is reported and compared with results from LILITA and CASCADE. The experimental data show two well-defined structures: The former is centered around the projectile Z value and the latter in the region of high Z where the evaporation residues are expected.

Two different calculations have been performed and are reported in Fig. 4. Dashed lines refer to the standard statistical-model calculations as already described. The continuous lines refer to model calculations in which the effects of compound-nucleus deformation are simulated following Ref. 23. These calculations are justified by the fact that the majority of the evaporation occurs at high angular momenta ($20-30\hbar$) of the emitting nucleus, where sizeable deformations are predicted by the rotating liquid drop model.[27] In statistical-model calculations, deformations are taken into account in calculating the yrast line. In this way also the level-density spin dependence is changed. Following Ref. 23, potentials with their radius increased by 10% have been used to simulate the effects of deformation in the particles evaporation.

It seems generally that the CASCADE code is better able to describe the evaporation residue distribution with respect to LILITA calculations. In the present case, the CASCADE calculations with the inclusion of deformation effects are able to reproduce the cross sections also for the lower Z of fusion distribution. However, statistical models predict evaporation residue distributions which are slightly shifted towards heavier Z with respect to the experimental ones. This may also be due to the fact that the tail of the bump in the $\sigma(Z)$ distribution centered

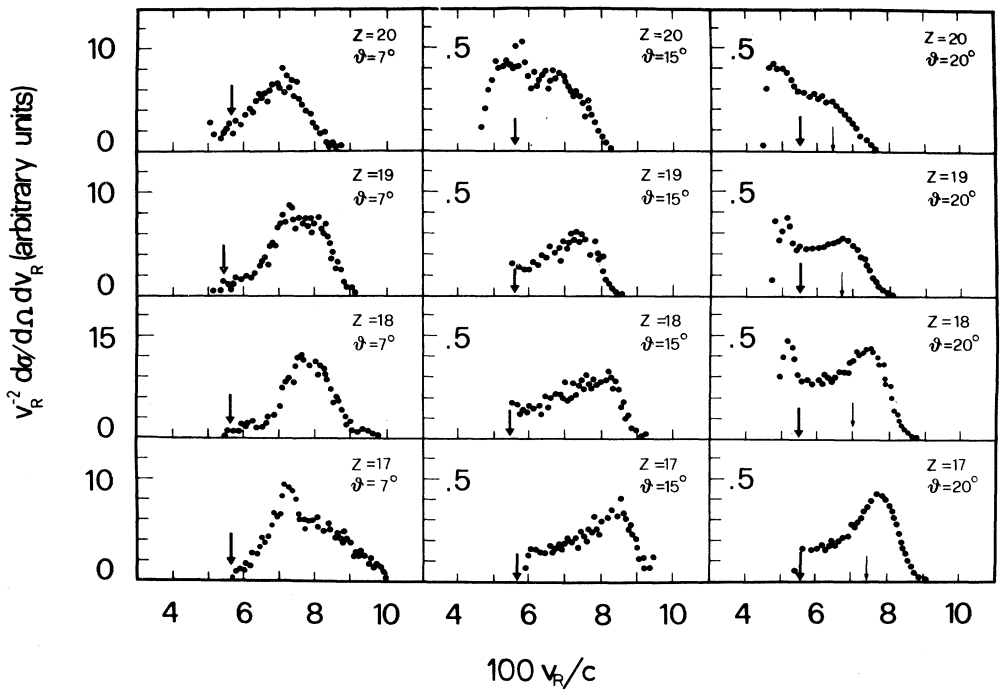

FIG. 3. As Fig. 2, but for fragments with $Z=20-17$. Thick arrows represent the expected velocity for complete fusion; thin ones, shown for the spectra at $\theta=20°$, represent the velocity corresponding to Coulomb repulsion energy in the case of binary fragmentation of the compound system.

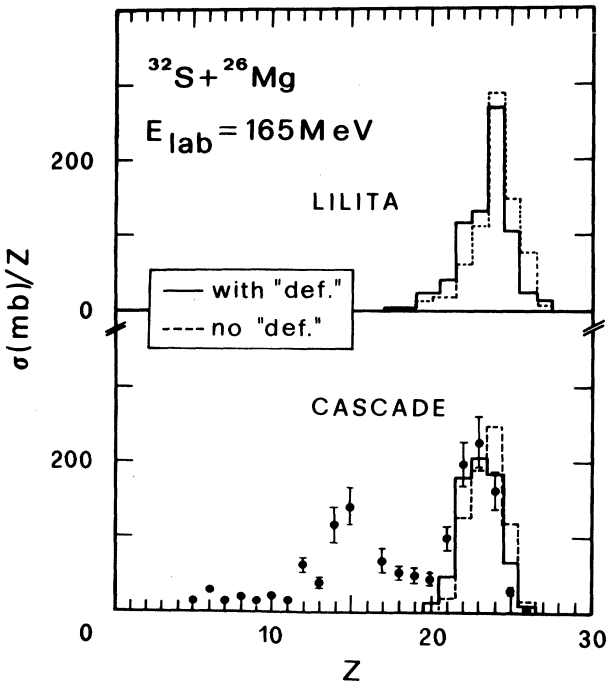

FIG. 4. Measured elemental distribution compared with predictions from statistical-model calculations from LILITA and CASCADE. The "def." indicates that deformations are accounted for in the statistical model. For details, see the text.

around the projectile Z value extends into the evaporation residue region. In this case the results from the comparison in Fig. 4 support the angular-distribution and velocity-distribution findings about the overlap of fusion and other reaction mechanisms for fragments with $Z=20-21$.

To derive the complete fusion cross sections, we summed the contributions of fragments with $Z=26$ to $Z=22$ contributions adding 70% of the yield for $Z=21$ and 40% for that of $Z=20$. The value of 730 ± 140 mb for the complete fusion cross section is found in this way, in agreement with the value of 800 ± 100 mb from Ref. 23. The results reported here confirm the findings of Refs. 19 and 23 about the decrease of the fusion cross section at these bombarding energies.

IV. BINARY REACTIONS

In this section, data are presented on the reaction products having atomic number lower than that ascribed to the fusion reaction ($Z=26-20$). Features of the reaction mechanisms competing with the fusion will be deduced by inspection of energy spectra and angular distributions with the aid of semiclassical models of inelastic collisions.

Velocity spectra for fragments with $Z=20-17$ have already been shown in Fig. 3; energy spectra for fragments with $Z=15-6$ are shown in Fig. 5. Arrows in Fig. 5 indicate the Coulomb repulsion energies between the detected fragment and its binary (undetected) partner. Coulomb energies have been calculated by assuming that the undetected fragments have atomic number $Z_4=Z_{CN}-Z_3$ and using mass values of the most naturally abundant isotopes. It can be seen that energy spectra are characterized by a broad bump having its maximum at an energy value slightly higher than the Coulomb energy one. This behavior is similar to that shown in Fig. 3 for heavier fragments. The grazing angle in the entrance channel for the $^{32}S+^{26}Mg$ reaction at 165 MeV is relatively forward ($\theta_{1/4}=13°$ in the labsystem), so that quasielastic contributions are seen in the energy (or velocity) spectra only for fragments with Z value close to that of the projectile ($Z=17-13$) detected at small angles. In general, fragment spectra show large damping of the kinetic energy.

The angular distributions of fragments with $Z=20-10$ are reported in Fig. 6. They show the well-known transition from forward peaking to isotropy as the net charge transfer is increased going towards reaction products lighter or heavier than the projectile. The flattening of the angular distributions is generally taken as an indication of long reaction times. This effect is associated, as in this case, to the complete relaxation of the relevant degree of freedom (kinetic energy, angular momentum, nuclear shape). These damped reaction mechanisms are those competing with fusion.

It seemed interesting to analyze further the spectra of fragments showing large damping of kinetic energy. To exclude any contribution from quasielastic reactions, spectra at $\theta_{lab}=20°$ were taken into account for $Z=20$ to $Z=17$; similarly, for $Z=15$ to $Z=6$ spectra at $\theta_{lab}=30°$ were chosen. The most probable total kinetic energies E_T as a function of the fragment Z are reported in Fig. 7. Corrections for the effect of sequential particle evapora-

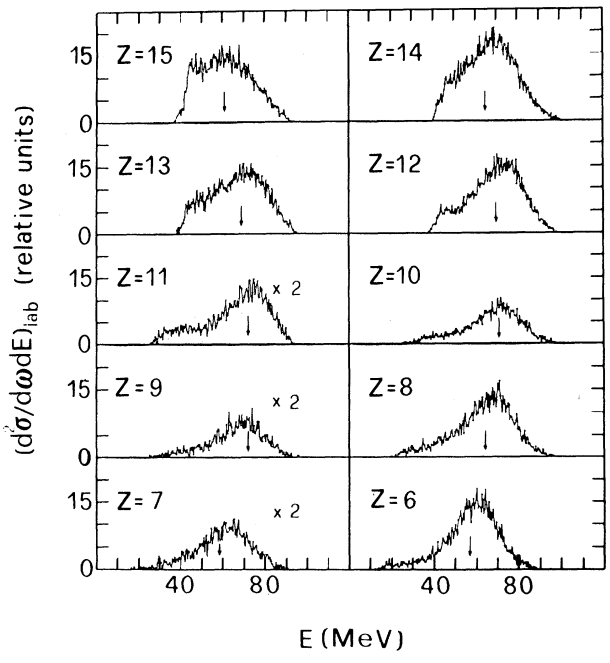

FIG. 5. Energy spectra of fragments with $Z=15-6$, taken at $\theta_{lab}=30°$. The arrows indicate the positions of Coulomb repulsion energy.

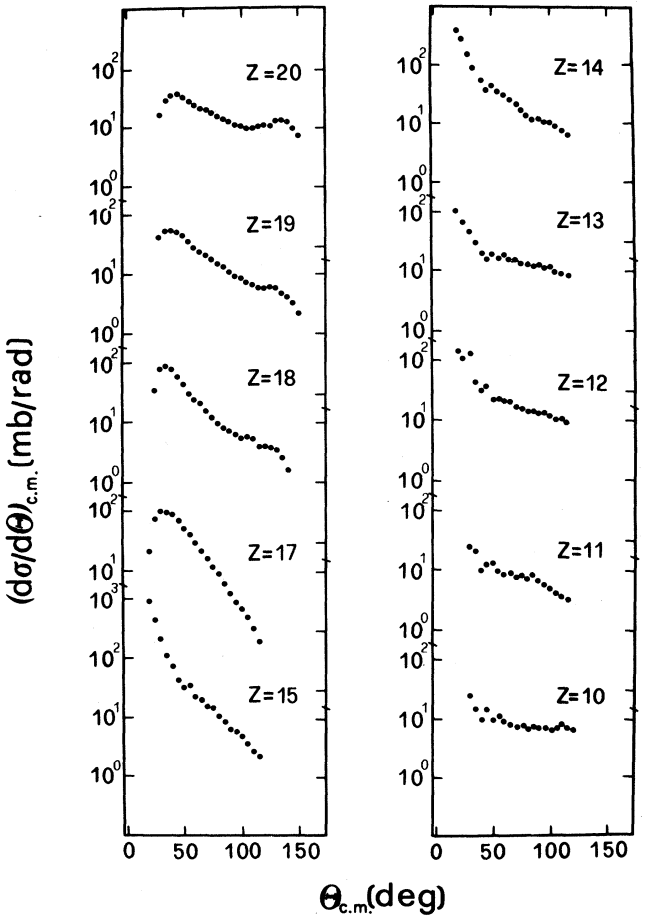

FIG. 6. Angular distributions of fragments with $Z=15-6$.

tion from the fragments have been made following the procedures of Refs. 28 and 29. To this end, an excitation energy partition between the reaction partners proportional to their mass ratio has been used. This assumption seems to be realistic in the present case because we are considering events which show almost complete energy relaxation.

The comparison of calculated Coulomb energies with the experimental E_T values in Fig. 7 shows that there is an underestimation of the kinetic energies of fragments with $Z=12-17$. In fact, it is well known that rotational energies as well as the attractive nuclear potential contribute to the kinetic energies at scission.

In a deeply inelastic collision it is assumed that kinetic energies of the fragments are directly related to the scission configuration of the dinuclear system approximated by two uniform spheres of radii R_3 and R_4 joined by a neck. The distance between the centers of two spheres is then

$$s=R_3+R_4+d \ , \tag{3}$$

where for R_3 and R_4 it is assumed that $R_i=1.2A_i^{1/3}$ and d is the neck length. The total kinetic energy of the dinuclear system at scission is

$$E_T=V_{\rm Coul}(s)+V_{\rm nucl}(s)+\frac{L_f(L_f+1)\hbar^2}{2\mu s^2} \ , \tag{4}$$

where μ is the reduced mass of exit channel and L_f is the exit-channel angular momentum. For L_f the sticking limit is assumed to be

$$L_f=\frac{\mu s^2 L_i}{\mu s^2+I_3+I_4} \ , \tag{5}$$

where L_i is the entrance-channel angular momentum and I_i are the fragment moments of inertia.

The rotation energy has been estimated following the model of Simbel and Abul-Magd.[30] In this model it is assumed that, within the window $l_{\rm cr}\le l\le l_{\rm graz}$ which contributes to inelastic processes, various partial waves have different weights depending on the overlap between the fragments. The average value of the angular momentum L_i populating the inelastic reaction is written as $L_i=\alpha l_{\rm cr}+(1-\alpha)l_{\rm graz}$. The parameter α expresses the degree of overlap between the two fragments and is defined as $\alpha=(N/N_{\rm max})^{1/2}$, where N is the number of protons transferred between the fragments, and $N_{\rm max}$ is the maximum possible number of protons transferred under conditions of maximum overlap at $l=l_{\rm cr}$. In our case we found $N_{\rm max}\approx 5$. This is consistent with the width of the peak in the elemental distribution centered around the projectile Z reported in Fig. 4.

For the nuclear potential $V_{\rm nucl}$, we have used proximity potential from Ref. 7, employed in the past in calculating fusion cross sections for the ^{32}S+Mg systems. In Fig. 7, the continuous curve shows the results of calculations assuming $l_{\rm cr}=35\hbar$, $l_{\rm graz}=53\hbar$, and the distance $s=8.4$ fm, which corresponds to a neck length of ≈ 1 fm. Total kinetic energies of binary fragments are well accounted for by the calculations as shown in Fig. 7, indicating that inelastic processes lie in the interaction region intermediate between the grazing distance (≈ 9 fm) and that

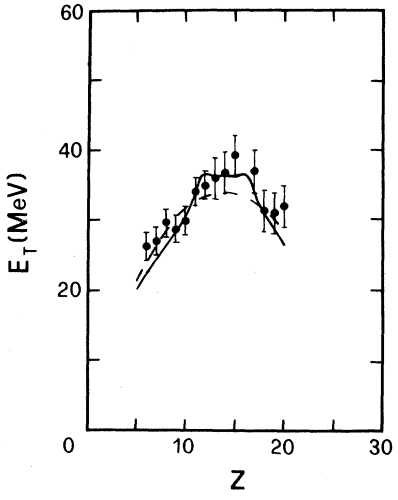

FIG. 7. Total kinetic energy of fragments vs Z. The dashed line corresponds to calculated Coulomb repulsion energies. The continuous line refers to calculation in which rotational energy and nuclear potential contribution are accounted for.

defined by the critical angular momentum for fusion ($R_{cr}=5.60$ fm[19]).

V. SUMMARY AND CONCLUSIONS

A detailed study of the fusion reaction and binary processes has been performed for the interaction of ^{32}S with ^{26}Mg at $E_{lab}=163.5$ MeV. The present results confirm the existence of a bombarding energy region where the fusion cross section σ_{fus} is strongly limited and decreases with $1/E_{cm}$. From the comparison of angular distributions and velocity spectra with predictions from statistical-model calculations, it appears that the complete fusion reaction populates exclusively fragments with $Z=26-22$. Other reaction mechanisms than the fusion contribute to the yield of residues with $Z=21$ and $Z=20$.

Angular distributions and total kinetic energies of lighter fragments ($Z \leq 20$) indicate that the main mechanism limiting fusion is a strong inelastic process. It presents nearly complete energy damping and angular distributions which indicate long interaction times. Total kinetic-energy calculations including estimates of the rotational energy and nuclear potential contributions reproduce the experimental data quite well.

ACKNOWLEDGMENTS

The authors wish to thank the Laboratori Nazionali di Legnaro for their kind hospitality and the technical support received during the experiment at the XTU-Tandem. Mr. S. Leotta, Mr. F. Librizzi, and Mr. D. Nicotra of the Istituto Nazionale di Fisica Nucleare (INFN), Section of Catania are thanked for their assistance during the measurements.

*Permanent address: Institute of Modern Physics, Lanzhou, China.

[1]B. Natowitz, M. N. Namboodiri, R. Eggers, P. Gonthier, K. Geoffroy, R. Hanus, C. Towsley, and K. Das, Nucl. Phys. **A277**, 477 (1977).

[2]H. Lehr, W. Bohne, K. Grabisch, H. Morgenstern, and W. Von Oertzen, Nucl. Phys. **A415**, 149 (1984).

[3]G. Rosner, G. Hlawatsch, B. Kolb, G. Doukellis, J. B. Natowitz, and J. h. Walcher, Nucl. Phys. **A385**, 174 (1982).

[4]Y. Nagashima, J. Schimizu, T. Nakagawa, Y. Fukuchi, W. Yokota, K. Furuno, M. Yamanouchi, S. M. Lee, N. X. Dai, and T. Mikumo, Phys. Rev. C **33**, 176 (1986).

[5]H. Dumont, B. Delaunay, J. Delaunay, D. M. De Castro Rizzo, M. Brondi, P. Cuzzocrea, A. D'Onofrio, R. Moro, M. Romano, and F. Terrasi, Nucl. Phys. **A435**, 301 (1985).

[6]D. Glas and U. Mosel, Nucl. Phys. **A237**, 429 (1975).

[7]C. Ngô, in Proceedings of the International Conference on Nuclear Physics, Florence, 1983, edited by P. Blasi and R. A. Ricci, Vol. II, p. 321.

[8]J. R. Birkelund, L. E. Tubbs, J. R. Huizenga, J. N. De, and D. Sperber, Phys. Rep. **56**, 107 (1979).

[9]P. Frobrich, Phys. Rev. **116**, 337 (1984).

[10]S. M. Lee, T. Matsuse, and A. Arima, Phys. Rev. Lett. **45**, 165 (1980).

[11]T. Matsuse, A. Arima, and S. M. Lee, Phys. Rev. C **26**, 2338 (1982).

[12]R. Vandenbosch, Phys. Lett. **87B**, 183 (1979).

[13]F. Saint Laurent, M. Conjeaud, S. Harar, J. M. Loiseaux, J. Menet, and J. B. Viano, Nucl. Phys. **A327**, 517 (1979).

[14]S. J. Sanders, R. R. Betts, I. Ahmad, K. T. Lesko, S. Saini, B. D. Wilkins, R. Videback, and B. K. Dichter, Phys. Rev. C **34**, 1746 (1986).

[15]J. Barrette, P. Braun-Munzinger, C. K. Gelbke, H. E. Wegner, Z. Zeidman, A. Gamp, H. L. Harney, and Th. Walcher, Nucl. Phys. **A279**, 125 (1977).

[16]G. Rosner, J. Pochodzalla, B. Heck, G. Hlawatsch, A. Miczaika, H. J. Rabe, R. Butsch, B. Kolb, and B. Sedelmeyer, Phys. Lett. **150B**, 87 (1985).

[17]D. Shapira, D. Digregorio, J. Gomez del Campo, R. A. Dayras, J. L. C. Ford, Jr., A. H. Snell, P. H. Stelson, R. G. Stokstad, and F. Pougheon, Phys. Rev. C **28**, 1148 (1983).

[18]R. Ritzka, W. Dunnweber, A. Glaesner, W. Hering, H. Puchta, and W. Trautmann, Phys. Rev. C **31**, 133 (1985).

[19]Sl. Cavallaro, Luo Yi Xiao, and M. L. Sperduto, Phys. Rev. C **32**, 1584 (1985).

[20]A. Moroni, I. Iori, Li Zu Yu, G. Prete, G. Viesti, F. Gramegna, and A. Dainelli, Nucl. Instrum. Methods, **225**, 57 (1984).

[21]J. Gomez del Campo and R. G. Stokstad, Oak Ridge National Laboratory Report ORNL/TM-7295, 1981; and LILITA 1, version of the code modified by A. D'Onofrio and J. Gomez del Campo, Saclay, 1986.

[22]F. Puhlhofer, Nucl. Phys. **A280**, 267 (1977).

[23]F. Puhlhofer, W. F. W. Schneider, F. Busch, J. Barrette, P. Braun-Munzinger, C. K. Gelbke, and H. E. Wegner, Phys. Rev. C **16**, 1010 (1977).

[24]J. Gomez del Campo, R. G. Stokstad, J. A. Biggerstaff, R. A. Dayras, A. H. Snell, and P. H. Stelson, Phys. Rev. C **19**, 2170 (1979).

[25]H. Morgenstern, W. Bohne, K. Grabisch, D. Kovar, and H. Lehr, Phys. Rev. Lett. **113B**, 463 (1982).

[26]Sl. Cavallaro, M. L. Sperduto, and Luo Yi Xiao, Nuovo Cimento A **100**, 603 (1988).

[27]S. Cohen, F. Plasil, and W. Swiatecki, Ann. Phys. (N.Y.) **82**, 557 (1974).

[28]Nguyen Van Sen, R. Darves-Blanc, J. C. Gondrand, and F. Merchez, Phys. Rev. C **27**, 194 (1983).

[29]P. Wastyn, H. Felmeir, F. Beck, M. Dworzecka, H. Genz, M. Mutterer, A. Richter, G. Schrieder, and J. P. Theobald, Nucl. Phys. **A332**, 445 (1979).

[30]M. H. Simbel and A. Y. Abul Magd, Z. Phys. A **294**, 277 (1980).